Photoelectron spectroscopy and the electronic structure of the uranyl tetrachloride dianion: $UO_2Cl_4^{2-}$

Phuong Diem Dau, Jing Su, Hong-Tao Liu, Dao-Ling Huang, Jun Li et al.

Citation: J. Chem. Phys. **137**, 064315 (2012); doi: 10.1063/1.4742062
View online: http://dx.doi.org/10.1063/1.4742062
View Table of Contents: http://jcp.aip.org/resource/1/JCPSA6/v137/i6
Published by the American Institute of Physics.

Photoelectron spectroscopy and the electronic structure of the uranyl tetrachloride dianion: $UO_2Cl_4^{2-}$

Phuong Diem Dau,[1] Jing Su,[2] Hong-Tao Liu,[1] Dao-Ling Huang,[1] Jun Li,[2,a)] and Lai-Sheng Wang[1,b)]
[1]*Department of Chemistry, Brown University, Providence, Rhode Island 02912, USA*
[2]*Department of Chemistry and Key Laboratory of Organic Optoelectronics and Molecular Engineering of Ministry of Education, Tsinghua University, Beijing 100084, China*

(Received 16 June 2012; accepted 19 July 2012; published online 10 August 2012)

The uranyl tetrachloride dianion ($UO_2Cl_4^{2-}$) is observed in the gas phase using electrospray ionization and investigated by photoelectron spectroscopy and relativistic quantum chemical calculations. Photoelectron spectra of $UO_2Cl_4^{2-}$ are obtained at various photon energies and congested spectral features are observed. The free $UO_2Cl_4^{2-}$ dianion is found to be highly stable with an adiabatic electron binding energy of 2.40 eV. *Ab initio* calculations are carried out and used to interpret the photoelectron spectra and elucidate the electronic structure of $UO_2Cl_4^{2-}$. The calculations show that the frontier molecular orbitals in $UO_2Cl_4^{2-}$ are dominated by the ligand Cl 3*p* orbitals, while the U–O bonding orbitals are much more stable. The electronic structure of $UO_2Cl_4^{2-}$ is compared with that of the recently reported $UO_2F_4^{2-}$ [P. D. Dau, J. Su, H. T. Liu, J. B. Liu, D. L. Huang, J. Li, and L. S. Wang, Chem. Sci. **3** 1137 (2012)]. The electron binding energy of $UO_2Cl_4^{2-}$ is found to be 1.3 eV greater than that of $UO_2F_4^{2-}$. The differences in the electronic stability and electronic structure between $UO_2Cl_4^{2-}$ and $UO_2F_4^{2-}$ are discussed. © *2012 American Institute of Physics*. [http://dx.doi.org/10.1063/1.4742062]

I. INTRODUCTION

The chemical and electronic properties of the actinyl ions remain an interesting research topic because of their relevance to the disposal of nuclear wastes. Considerable research efforts have been devoted to understanding the electronic structures of the actinyls and the actinide-oxygen bonding properties in the condensed phase.[1–5] The uranyl dication (UO_2^{2+}) exists widely in uranium compounds,[6] and its electronic structure and bonding properties have been reviewed recently by Denning.[7] In UO_2^{2+}, the U atom forms two strong U≡O triple bonds with a linear geometry ($D_{\infty h}$, $^1\Sigma_g^+$).[7–10] The occupied frontier bonding molecular orbitals (MOs) of UO_2^{2+} (σ_u, σ_g, π_g, and π_u) are mainly oxygen based, with the σ_u orbital being the highest occupied MO (HOMO). The lowest unoccupied MOs (LUMOs) are U-based $5f_\delta$ and $5f_\phi$ orbitals, which do not participate in chemical bonding with the O atoms in UO_2^{2+} due to symmetry constraints. The uranyl ions are usually coordinated equatorially by a variety of ligands, which have weaker interactions with U through the d- and f-type LUMOs. The U-ligand interactions can, in turn, significantly influence the electronic structure and bonding properties of UO_2^{2+}.[7,11–16] However, there is generally a scarce of experimental data about the uranyl-ligand interactions. We have recently studied the isolated $UO_2F_4^{2-}$ species by combining photoelectron spectroscopy (PES) and *ab initio* calculations, revealing that the U–F bonding and the electrostatic repulsion from the F^- ligands weaken the axial U–O bonds.[17] The calculated U–O bond length in $UO_2F_4^{2-}$ at the coupled-cluster with single and double and perturbative triple excitations (CCSD(T)) level is about 1.81 Å, much longer than that in UO_2^{2+} (1.72 Å).[18,19]

The uranyl tetrachloride dianion, $UO_2Cl_4^{2-}$, is also an important uranyl complex in the condensed phase and has been the subject of detailed optical spectroscopy and theoretical studies both in the solid state as a $Cs_2UO_2Cl_4$ salt and in solutions.[11–15,20–26] However, accurate interpretations of the optical spectra of $UO_2Cl_4^{2-}$ in the condensed environments remain a challenging task in computational actinide chemistry.[16,18,26–28] For instance, the explanation of the spectroscopic data of crystallized $Cs_2UO_2Cl_4$ still relies on empirical models or approximate qualitative analyses.[25,29] Furthermore, due to prohibitive computational cost, high-level *ab initio* quantum chemistry calculations can only be applied to isolated actinyl species, such as UO_2^{2+}, $UO_2Cl_4^{2-}$, and $NpO_2Cl_4^{2-}$.[30–32] Gas-phase spectroscopy provides a unique opportunity to obtain experimental data without perturbation from the environmental effects in the condensed phases, allowing direct comparisons with high-level *ab initio* calculations. Previously, only one gas-phase vibrational spectroscopy study of singly charged uranyl halide anions has been reported.[33] We are interested in probing the electronic structures of actinyl complexes using electrospray ionization (ESI) and PES in the gas phase. Following our recent work on $UO_2F_4^{2-}$, here we report the observation and PES of the isolated tetrachloride dianion, $UO_2Cl_4^{2-}$. We find that $UO_2Cl_4^{2-}$ is even more electronically stable with an adiabatic electron binding energy (ADE) of 2.40 eV. Both density function theory (DFT) and wavefunction-based *ab initio* calculations are performed to help interpret the PES data and elucidate the electronic structure and bonding in

a)E-mail: junli@mail.tsinghua.edu.cn.
b)lai-sheng_wang@brown.edu.

$UO_2Cl_4^{2-}$. Significant differences in the electronic structure and bonding are found between the two tetrahalide dianions. The PES data of $UO_2Cl_4^{2-}$, as well as the recently reported data for $UO_2F_4^{2-}$,[17] provide valuable experimental results for benchmarking theoretical methods.

II. EXPERIMENTAL AND THEORETICAL METHODS

A. Electrospray ionization and photoelectron spectroscopy

The experiment was carried out using our ESI-PES apparatus, which was described in detail previously.[34] The only modification was the shortening of the electron flight tube from 4.0 m to 2.5 m, resulting in a slight decrease of electron energy resolution.[35] Briefly, the $UO_2Cl_4^{2-}$ anion was produced by electrospray of a 1 mM solution of UCl_4 in acetonitrile with a trace amount of water. A radio frequency-only quadrupole device guided the anions from the ESI source into a Paul trap operated at room temperature, where anions were accumulated for 0.1 s before being pulsed into the extraction zone of a time-of-flight mass spectrometer. Under our ESI condition, strong $UO_2Cl_4^{2-}$ dianion signals were produced, presumably as a result of oxidation reactions of UCl_4 with O_2 and water during the ESI. The $UO_2Cl_4^{2-}$ anions were selected by a mass gate and decelerated before being intercepted by a laser beam in the detachment region of a magnetic-bottle photoelectron analyzer. Three different lasers were used for the PES experiment in the current work: 157 nm (7.866 eV) from an F_2 excimer laser, 213 nm (5.821 eV) and 245 nm (5.061) from a dye laser, and 266 nm (4.661 eV) from a Nd:YAG laser. The PES spectra were calibrated using the known spectra of Au^- and I^-. The Au^- anion was produced by electrospraying a pyridine solution of PPh_3AuCl with $NaSCH_3$ and a trace amount of CH_3OH.[36] The I^- anion was produced from a 0.1 mM NaI solution in a mixed water-methanol solution. The electron kinetic energy resolution of the current magnetic-bottle photoelectron analyzer with the shortened electron flight tube was about 3%, i.e., 30 meV for 1 eV electrons.[35]

B. Theoretical and computational methods

Theoretical studies were carried out using both DFT and *ab initio* wavefunction theory (WFT) methods. DFT calculations were carried out on the $UO_2Cl_4^{2-}$ dianion and $UO_2Cl_4^-$ monoanion using the generalized gradient approximation with the Perdew-Burke-Ernzerhof (PBE) exchange-correlation functional[37] and the hybrid functional known as B3LYP (Ref. 38) as implemented in the Amsterdam Density Functional (ADF 2010.01) program.[39–41] The Slater basis sets with the quality of triple-ζ plus two polarization functions (TZ2P) (Ref. 42) were used, with the frozen core approximation applied to inner shells, $[1s^2\text{-}5d^{10}]$ for U, $[1s^2]$ for O, and $[1s^2\text{-}2p^6]$ for Cl. The scalar relativistic (SR) and spin-orbit (SO) coupling effects were taken into account by the zero-order regular approximation (ZORA).[43] Geometries were fully optimized at the SR-ZORA level and single-point energy calculations were performed with inclusion of the SO effects via the SO-ZORA approach.

To compare with the experimental results, *ab initio* WFT calculations were done on $UO_2Cl_4^{2-}$ using more advanced electron correlation methods in the MOLPRO 2008.1 program.[44] Both the CCSD(T) and complete-active-space self-consistent field (CASSCF) methods were used in these calculations. The geometry of $UO_2Cl_4^{2-}$ was optimized at the level of CCSD(T) with SR effects included. Single-point CCSD(T) energies of the ground and excited states of $UO_2Cl_4^-$ were calculated at the optimized SR-CCSD(T) geometry of $UO_2Cl_4^{2-}$, generating accurate state-specific SR energies for all the states. The electron detachment energies corresponding to one-electron transitions from the closed-shell ground state of $UO_2Cl_4^{2-}$ to the ground and excited states of $UO_2Cl_4^-$ were obtained using the CASSCF/CCSD(T)/SO approach,[17,45–48] which has been shown to generate accurate excitation energies for molecules containing heavy elements.[17,32,49] In this approach, the SO splittings were treated as a perturbation to the SR state energies and were calculated on the basis of CASSCF wavefunctions with the diagonal matrix elements replaced by the individual CCSD(T) state energies. SO splitting was calculated by using a state-interacting method with SO pseudopotentials. We also used the CASSCF/CR-EOM-CCSD(T)/SO approach,[17,32,49] where the completely renormalized equation-of-motion CCSD(T) (CR-EOM-CCSD(T),[50]) energies, derived from the EOM-CCSD calculations with completely renormalized EOM-CCSD(T) corrections as implemented in NWChem 6.0, were used as the diagonal elements.[51] In this approach, the CR-EOM-CCSD(T) calculations were performed on the monoanion at the optimized CCSD(T) geometry of the dianion to obtain the vertical energies of the excited states, with the CCSD(T) energy of the first state used as a reference. In the MOLPRO and NWChem calculations, we used the Stuttgart energy-consistent relativistic pseudopotential ECP60MWB (U),[52–55] and the corresponding valence triple-ζ basis sets aug-cc-pVTZ for O and Cl.[56,57] These basis sets and pseudopotential are shown to produce reasonably accurate results for excitation energies of actinide complexes.[17,32,49,58]

III. EXPERIMENTAL RESULTS

Figure 1 displays the PES spectra of $UO_2Cl_4^{2-}$ at four different photon energies. The 157 nm spectrum (Fig. 1(d)) reveals congested detachment features between 2 and 5 eV binding energies, as labeled from X to F. These features are all fairly broad, owing to either a large geometric change from the dianion to the monoanion states and/or overlaps of multiple detachment transitions. Thus, the labels are for the sake of discussion and cannot be viewed as representing single electronic transitions, as usually done. At 213 nm (Fig. 1(c)), bands X and A are better resolved. However, the relative intensities of bands B–F are significantly reduced, due to the repulsive Coulomb barrier (RCB) expected for a dianion.[59] The RCB cuts off higher binding energy (low kinetic energy) features, when detachment photon energies ($h\nu$) are decreased. With a sharp cutoff, one can estimate the

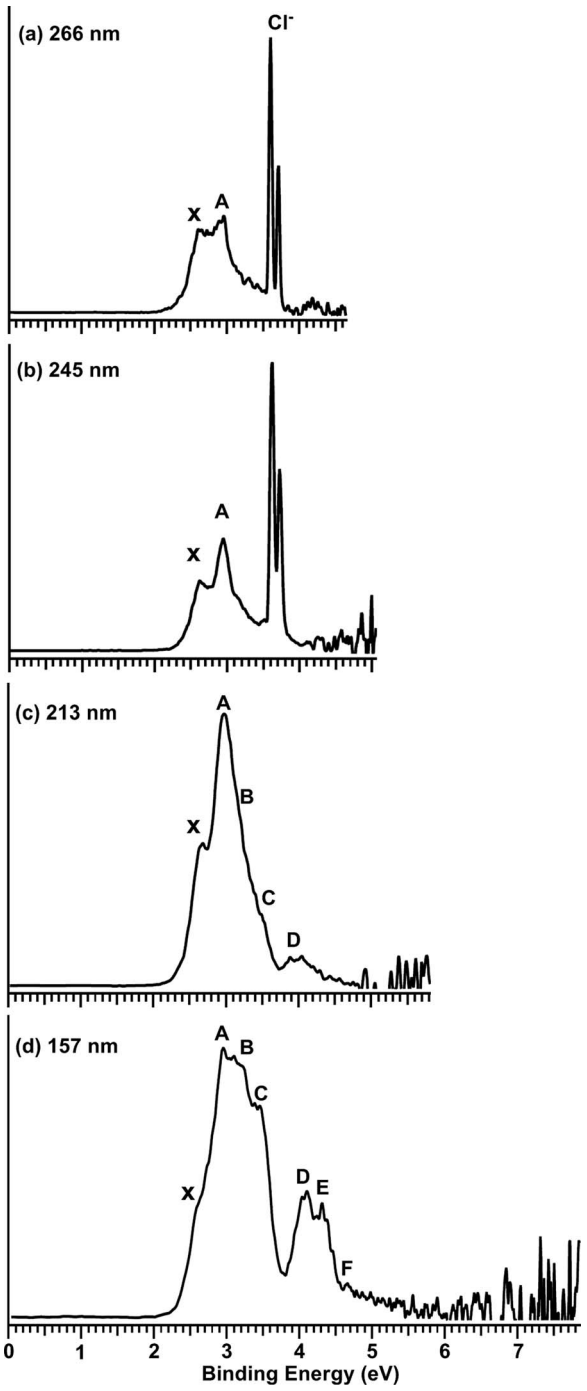

FIG. 1. Photoelectron spectra of $UO_2Cl_4^{2-}$ at (a) 266 nm (4.661 eV), (b) 245 nm (5.061 eV), (c) 213 nm (5.821 eV), and (d) 157 nm (7.866 eV).

magnitude of the RCB (hν—cutoff). However, because of electron tunneling,[60] the RCB cannot define a sharp cutoff threshold and its height can only be estimated from the PES spectra at different photon energies. The 213 nm spectrum suggests that band D (vertical detachment energy (VDE): 4.1 eV) is probably near the barrier top, yielding a RCB < 2 eV.

At 245 nm (Fig. 1(b)), band D is cut off and the relative intensities of bands A–C are further reduced, consistent with the RCB estimated from the 213 nm spectrum. The sharp and intense double peaks around 3.6 eV in the 245 nm spectrum are due to detachment of Cl^-, originated from photodissociation of the $UO_2Cl_4^{2-}$ parent dianion at 245 nm through the reaction: $UO_2Cl_4^{2-} \rightarrow UO_2Cl_3^- + Cl^-$. The electron binding energies of the $UO_2Cl_3^-$ fragment are too high for its photodetachment to be observed at 245 nm.[61] Similar photodissociation is also observed at 266 nm (Fig. 1(a)), as shown by the observation of the sharp Cl^- detachment signals. The photodissociations are most likely due to resonant absorption of a detachment photon, which does not seem to occur at 213 or 157 nm. At 266 nm, feature A is partially cut off at about 3 eV binding energy, which suggests a RCB of ~1.7 eV (4.661 eV–3 eV). This RCB is lower than that estimated for $UO_2F_4^{2-}$ previously,[17] in agreement with the smaller size and the higher intramolecular Coulomb repulsion of the tetrafluoride dianion. The ADE and VDE for the ground state transition from $UO_2Cl_4^{2-}$ to $UO_2Cl_4^-$ are determined from the X band as 2.40 ± 0.08 eV and 2.62 ± 0.05 eV, respectively. The VDE is measured from the maximum of band X. Because no vibrational structure is resolved, the ADE is determined by drawing a straight line along the leading edge of band X and then adding the instrumental resolution to the intersection to the binding energy axis. The ADE of $UO_2Cl_4^{2-}$ is much larger than that of $UO_2F_4^{2-}$ (1.10 eV),[17] indicating that $UO_2Cl_4^{2-}$ is highly electronically stable in the gas phase.

TABLE I. Observed adiabatic (ADE) and vertical (VDE) detachment energies for $UO_2Cl_4^{2-}$ compared to calculations at different levels of theory.[a] All energies are in eV.

		B3LYP		CCSD(T)
	Exp.	SR	SO	SR
ADE	2.40 ± 0.08	1.75	1.80	2.58
VDE	2.62 ± 0.05	1.77	1.83	2.61

[a]The ADE and VDE correspond to one-electron detachment from the $1a_{2g}$ orbital (see Figs. 2 and 3).

IV. THEORETICAL RESULTS

The calculated first ADE and VDE for $UO_2Cl_4^{2-}$ at the DFT/B3LYP and CCSD(T) levels are compared with the experimental data in Table I. The DFT/B3LYP binding energies are significantly lower than the experimental values, most likely due to the self-interaction error. The underestimated electronic binding energies of highly charged anions at DFT levels were also observed in our previous studies of $Pt(CN)_6^{2-}$ (Ref. 62) and $UO_2F_4^{2-}$.[17] In as much as the frontier MOs are mainly from Cl 3*p* orbitals in both $UO_2Cl_4^{2-}$ and $UO_2Cl_4^-$, the SO relativistic effects are expected to be small.[63] At the DFT/B3LYP level, inclusion of the SO coupling effects only improves the ADE and VDE of $UO_2Cl_4^{2-}$ by ~0.05 eV. The calculated ADE (2.58 eV) and VDE (2.61 eV) at the SR-CCSD(T) level are in much better agreement with the experiment. In particular, the VDE is in excellent agreement with the experiment, although without SO corrections the SR-CCSD(T) method still overestimates the ADE for $UO_2Cl_4^{2-}$ by about 0.2 eV, which is similar to our previous finding for the case of $UO_2F_4^{2-}$.[17]

The optimized ground-state geometrical parameters of $UO_2Cl_4^{2-}$ and $UO_2Cl_4^-$ at the SR level are given in Table II. Upon electron detachment from $UO_2Cl_4^{2-}$, both

TABLE II. Optimized geometrical parameters of $UO_2Cl_4^{2-}$ and $UO_2Cl_4^{-}$ at the scalar relativistic level.

			DFT/PBE[a]		DFT/B3LYP		CCSD(T)	
	Sym	GS	U–O (Å)	U–Cl (Å)	U–O (Å)	U–Cl (Å)	U–O (Å)	U–Cl (Å)
$UO_2Cl_4^{2-}$	D_{4h}	$^1A_{1g}$	1.807	2.734	1.809	2.766	1.766	2.735
$UO_2Cl_4^{-}$	D_{4h}	$^2A_{2g}$	1.794	2.705	1.798	2.737	1.760	2.690

[a]DFT/PBE method erroneously gives a $^2A_{2u}$ state as the ground state (GS) of $UO_2Cl_4^{-}$, lower than the $^2A_{2g}$ state by 0.12 eV, which is within the error of the DFT method used. The two states correspond to one-electron detachment from the $2a_{2u}$ and $1a_{2g}$ orbitals of $UO_2Cl_4^{2-}$, respectively. See Figs. 2 and 3.

DFT and CCSD(T) calculations show that the U–Cl bonds are shortened by about 0.03–0.04 Å and the U–O bonds are slightly shortened by about 0.01 Å in the $UO_2Cl_4^{-}$ monoanion.

The occupied valence MO levels for $UO_2Cl_4^{2-}$ are shown in Fig. 2 with SR and SO effects included, and details of the calculated VDEs for all the MOs by DFT/PBE can be found in Table III. Among these MOs, the $1e_u$ and $2e_u$ orbitals display strong SO effects (Fig. 2) due to contributions of the U $5f\pi$ orbitals to the former and U $5f\phi$ and $6p$ orbitals to the latter. The $1a_{1g}$ $1e_g$, $1e_u$, and $1a_{2u}$ MOs are the U–O bonding orbitals, and the remaining MOs are primarily Cl $3p$ type orbitals (Table III). The three-dimensional iso-surface contours of the occupied MOs for $UO_2Cl_4^{2-}$ from DFT calculations are presented in Fig. 3.

The calculated VDEs from all the valence MOs using the CASSCF/CCSD(T)/SO and CASSCF/CR-EOM-CCSD(T)/SO methods are given in Table IV. The simulated PES spectra of $UO_2Cl_4^{2-}$ using these calculated VDEs are shown in Fig. 4, where they are compared with the experimental spectrum at 157 nm.

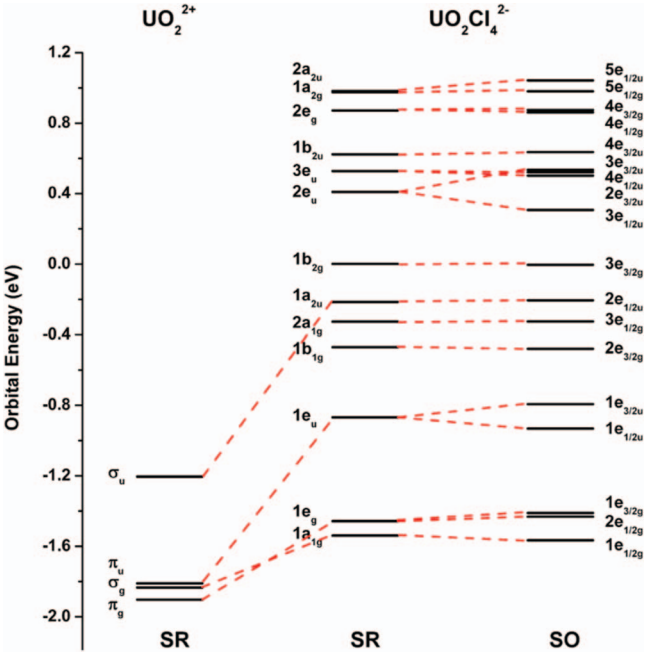

FIG. 2. The SR and SO energy levels of the frontier occupied orbitals of $UO_2Cl_4^{2-}$ calculated at the DFT/PBE level. The $1a_{1g}$, $1e_g$, $1e_u$, and $1a_{2u}$ orbitals correspond to U–O bonding orbitals in UO_2^{2+} and all the other orbitals mainly belong to Cl $3p$ lone pairs.

V. THE ELECTRONIC STRUCTURE OF $UO_2Cl_4^{2-}$ AND COMPARISON WITH EXPERIMENT

A. Valence molecular orbitals of $UO_2Cl_4^{2-}$

Consistent with early DFT calculations,[7] the seven highest energy orbitals of the isolated $UO_2Cl_4^{2-}$ dianion are primarily centered on the chloride ligands (Table III). The bonding orbitals (σ_u, σ_g, π_g, and π_u) of the UO_2^{2+} moiety contribute to the low energy orbitals of $UO_2Cl_4^{2-}$, $1a_{1g}$, $1e_g$, $1e_u$, and $1a_{2u}$ (Table III and Fig. 2). All the valence orbitals (Fig. 3) show σ and π interactions between UO_2^{2+} and the Cl^- ligands except $1a_{2g}$, $2e_g$, $1b_{2u}$, and $2e_u$, which are essentially pure Cl $3p$ orbitals. There are π and σ bonding interactions between the non-bonding doubly degenerate U $6d$ δ_g orbitals and the Cl $3p_{x,y}$ orbitals, resulting in the $1b_{2g}$ and $1b_{1g}$ orbitals with ~11% contribution from the U $6d$ δ_g orbital. The pair of $1a_{2u}$ and $2a_{2u}$ orbitals show π bonding and anti-bonding interactions, where the UO_2^{2+} σ_u orbital has an in-phase and out-of-phase mixing with the Cl $3p_z$ orbitals in the equatorial plane, respectively. These two orbitals with a_{2u} symmetry also have ~5% contribution from the U $6p$ semicore orbitals. At the SR-DFT/PBE level, the

TABLE III. Calculated VDEs and the corresponding spinors of $UO_2Cl_4^{2-}$ from the SO-DFT/PBE level.

VDE#	VDE (eV)	Spinor		Main component of SR MOs
1	2.62[a]	$5e_{1/2u}$	$2a_{2u}$	Cl $3p$
2	2.68	$5e_{1/2g}$	$1a_{2g}$	Cl $3p$
3	2.79	$4e_{3/2g}$	$2e_g$	Cl $3p$
4	2.80	$4e_{1/2g}$	$2e_g$	Cl $3p$
5	3.03	$4e_{3/2u}$	$1b_{2u}$	Cl $3p$
6	3.13	$3e_{3/2u}$	$2e_u$	Cl $3p$
7	3.14	$4e_{1/2u}$	$3e_u$	Cl $3p$
8	3.16	$2e_{3/2u}$	$3e_u$	Cl $3p$
9	3.36	$3e_{1/2u}$	$2e_u$	Cl $3p$
10	3.67	$3e_{3/2g}$	$1b_{2g}$	Cl $3p$
11	3.87	$2e_{1/2u}$	$1a_{2u}$	U–O σ_u
12	3.99	$3e_{1/2g}$	$2a_{1g}$	Cl $3p$
13	4.14	$2e_{3/2g}$	$1b_{1g}$	Cl $3p$
14	4.46	$1e_{3/2u}$	$1e_u$	U–O π_u
15	4.60	$1e_{1/2u}$	$1e_u$	U–O π_u
16	5.07	$1e_{3/2g}$	$1e_g$	U–O π_g
17	5.10	$2e_{1/2g}$	$1e_g$	U–O π_g
18	5.23	$1e_{1/2g}$	$1a_{1g}$	U–O σ_g

[a]The VDE_1 calculated at SO-DFT/PBE level is 1.26 eV, which is underestimated relative to the experimental value. All VDEs listed are shifted by 1.36 eV to facilitate comparison with the experiment.

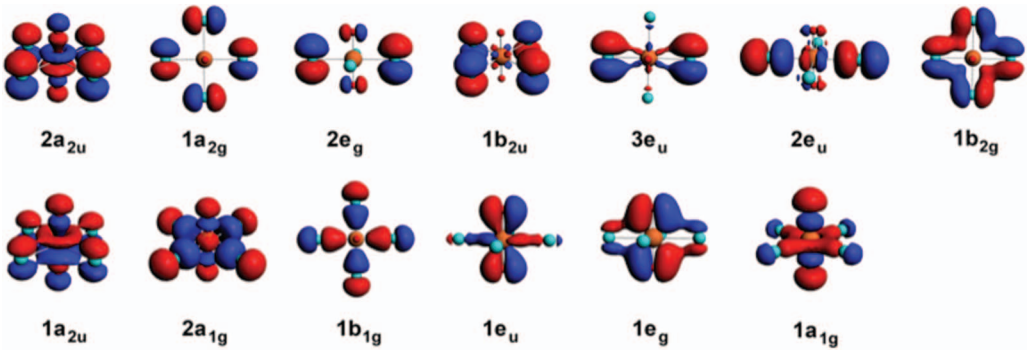

FIG. 3. The contour diagrams of the occupied valence orbitals of $UO_2Cl_4^{2-}$ at the DFT/PBE level. The $2a_{2u}$ and $1a_{2g}$ orbitals are close in energy and compete for the HOMO.

$2a_{2u}$ orbital is nearly degenerate with the nonbonding $1a_{2g}$ orbital composed of pure Cl $3p$. Even with the inclusion of additional SO relativistic effects in the DFT calculations, the first two highest occupied MOs of $UO_2Cl_4^{2-}$, $2a_{2u}$ and $1a_{2g}$, remain close in energy (Fig. 2). In addition, the UO_2^{2+} σ_g orbital has a σ bonding interaction with Cl $3p_{x,y}$ in the $1a_{1g}$ orbital, where the U $6d_\sigma$ has a small net overlap with the Cl $3p_{x,y}$ in the equatorial plane. The U $7s$ orbital contributes to the weak σ bonding in the $2a_{1g}$ orbital with less than 2% contribution. Finally, the non-bonding U $5f\phi_u$ orbital has a very small overlap with the Cl $3p_{x,y}$ in the $3e_u$ orbital.

B. Comparison with experiment

Upon removal of one valence electron, theoretical calculations at the DFT/B3LYP and CCSD(T) levels give the ground state of $UO_2Cl_4^-$ as $^2A_{2g}$ (Table II). This corresponds to electron detachment from the nonbonding $1a_{2g}$ orbital of pure Cl $3p$ character. This explains why all the U–O and U–Cl bond lengths do not change significantly between the ground states of the dianion and monoanion (Table II). The slightly shorter bond lengths in the $UO_2Cl_4^-$ monoanion are mainly due to the reduced intramolecular Coulomb repulsion.

TABLE IV. Calculated VDEs and the corresponding MOs of $UO_2Cl_4^{2-}$ at the CASSCF/CCSD(T)/SO and CASSCF/CR-EOM-CCSD(T)/SO levels.

	CASSCF/ CCSD(T)/SO		CASSCF/CR-EOM-CCSD(T)/SO	
VDE#	VDE (eV)	MOs (SR)	VDE (eV)	MOs (SR)
1	2.61	$1a_{2g}$	2.61	$1a_{2g}$
2	2.85	$2a_{2u}$	2.63	$2a_{2u}$
3	2.89	$2e_g$	2.66	$3e_u$
4	2.89	$2e_g$	2.68	$2e_g$
5	2.93	$2e_u$	2.68	$2e_g$
6	3.09	$3e_u$	2.77	$3e_u$
7	3.09	$3e_u$	2.90	$1b_{2u}$
8	3.14	$1b_{2u}$	2.90	$2e_u$
9	3.26	$2e_u$	3.12	$2e_u$
10	3.87	$1b_{2g}$	3.54	$1b_{2g}$
11	4.09	$2a_{1g}$	3.86	$2a_{1g}$
12	4.25	$1a_{2u}$	4.01	$1b_{1g}$
13	4.26	$1b_{1g}$	4.16	$1a_{2u}$
14	5.01	$1e_u$	4.99	$1e_u$
15	5.24	$1e_u$	5.21	$1e_u$
16	5.79	$1a_{1g}$	5.79	$1a_{1g}$
17	5.88	$1e_g$	5.91	$1e_g$
18	5.93	$1e_g$	5.96	$1e_g$

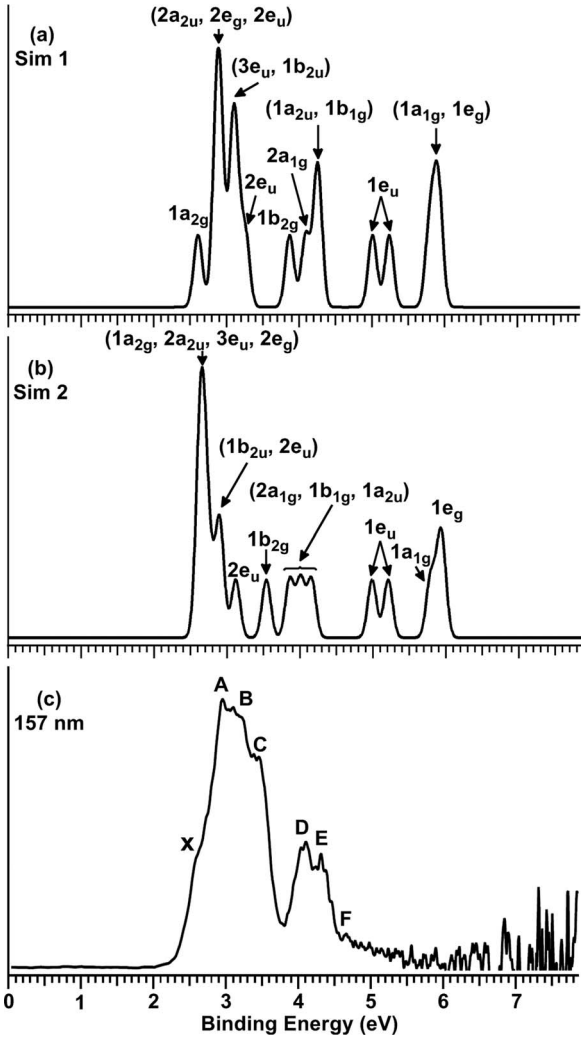

FIG. 4. Simulated photoelectron spectra of $UO_2Cl_4^{2-}$ from (a) CASSCF/CCSD(T)/SO calculations and (b) CASSCF/CR-EOM-CCSD(T)/SO calculations, in comparison with the 157 nm experimental data. The simulated spectra were generated by fitting a Gaussian of 0.06 eV width and unit area to each calculated VDE. The Gaussian width is chosen to be comparable to instrumental resolution at 157 nm. See Table IV for the detailed detachment channels.

The observed ADE of 2.40 eV indicates that $UO_2Cl_4^{2-}$ is a highly stable dianion in the gas phase. As seen in Table I, DFT calculations with or without SO effects significantly underestimate the electronic stability of the $UO_2Cl_4^{2-}$ dianion by ~0.6 eV. The SR-CCSD(T) calculation yields a better ADE (2.58 eV) and an excellent VDE (2.61 eV) for $UO_2Cl_4^{2-}$, compared to the experimental values of 2.40 and 2.62 eV, respectively. The difference between the CCSD(T) and experimental ADE is likely due to high-order electron correlation and truncation errors of the atomic basis sets used.

The calculated VDEs at the CASSCF/CCSD(T)/SO and CASSCF/CR-EOM-CCSD(T)/SO levels (Table IV) are fitted with Gaussians to yield the simulated PES spectra in Fig. 4, where they are compared with the 157 nm experimental spectrum. The two levels of theory give similar spectral patterns with some slight energy differences in a few detachment channels. The simulated spectrum at the CASSCF/CCSD(T)/SO level is in excellent qualitative agreement with the experimental data, owing to the single-excitation characters of the detachment transitions and the specifically optimized reference wavefunction in the CCSD(T) calculations. In addition to the detachment from the $1a_{2g}$ orbital, which gives the ground state transition (X), electron detachments from the $2a_{2u}$, $2e_g$, $2e_u$, $3e_u$, and $1b_{2u}$ orbitals result in the congested bands A, B, C. Following a small energy gap, detachments from the $1b_{2g}$, $2a_{1g}$, $1a_{2u}$, and $1b_{1g}$ orbitals give rise to bands D and E. All these orbitals are Cl based and are expected to have higher relative detachment cross sections. Even the primarily U–O $1a_{2u}$ orbital in this group contains significant contributions from Cl p_z (Fig. 3). Detachments from the primarily UO_2^{2+}-based $1e_u$ orbitals are expected to have lower relative cross sections and should correspond to the weak signals around 5 eV (Fig. 4(c)). The VDEs for detachments from the UO_2^{2+} $1a_{1g}$ and $1e_g$ orbitals are too high and are cut off by the RCB in the 157 nm spectrum. The overall agreement between the CASSCF/CCSD(T)/SO calculations and the PES data for $UO_2Cl_4^{2-}$ seems to be better than in the case of $UO_2F_4^{2-}$ at the same level of theory.[17]

VI. DISCUSSION

A. The electronic structure of $UO_2Cl_4^{2-}$ and intramolecular electrostatic interactions: $UO_2Cl_4^{2-}$ vs. $UO_2F_4^{2-}$

The measured ADE of 2.40 eV for $UO_2Cl_4^{2-}$ is 1.3 eV higher than that of $UO_2F_4^{2-}$.[17] This large difference in electronic stability between the two dianions reflects the difference in their electronic structures, which are strongly influenced by the intramolecular electrostatic interactions. Both uranyl halide dianions have the same D_{4h} symmetry and similar valence MOs, but the ordering of their valence MOs is very different: the frontier MOs of $UO_2F_4^{2-}$ are dominated by the U–O bonding orbitals of the UO_2^{2+} moiety,[17] while those of $UO_2Cl_4^{2-}$ are mainly from the Cl 3*p* orbitals (Figs. 2 and 3). Specifically, the ground state PES band of $UO_2Cl_4^{2-}$ arises from electron detachment from a nonbonding Cl 3*p* orbital ($1a_{2g}$, Fig. 3), while the HOMO of $UO_2F_4^{2-}$ comes from the σ_u orbital of UO_2^{2+}. This difference in the ordering of valence MOs is due to the intramolecular electrostatic interactions and the strength of the U-ligand interactions in the two uranyl tetrahalide dianions. Because the U–F bond lengths (2.23 Å) (Ref. 17) in $UO_2F_4^{2-}$ are much shorter than the U–Cl bond lengths (2.73 Å, Table I) in $UO_2Cl_4^{2-}$, the intramolecular Coulomb repulsion should be stronger in $UO_2F_4^{2-}$. This is reflected in their respective RCBs: the observed RCB in $UO_2F_4^{2-}$ was estimated to be ~2.0 eV,[17] while that in $UO_2Cl_4^{2-}$ is estimated to be ~1.7 eV in the current study. The high ADE of $UO_2Cl_4^{2-}$ is attributed to the high electron binding energy of the Cl^- ligands and the smaller intramolecular Coulomb repulsion. On the other hand, the low ADE of $UO_2F_4^{2-}$ is presumably due to its smaller size and the increased intramolecular Coulomb repulsion in the dianion, as well as the strong U–F interactions (*vide infra*).

B. The U–Cl bond length changes between $UO_2Cl_4^{2-}$ and $UO_2Cl_4^{-}$: Comparison with $UO_2F_4^{2-/1-}$

As shown in Table II, both DFT and CCSD(T) calculations show that the U–Cl bond lengths in $UO_2Cl_4^{2-}$ are about 2.73 Å, while the U–O bond lengths depend upon the computational methods. Because DFT calculations tend to overestimate the intramolecular Coulomb repulsion,[17] the U–O bond length of 1.766 Å by CCSD(T) is more reliable. It is noteworthy that both the DFT and CCSD(T) calculations show that the geometrical changes upon electron detachment are rather different for $UO_2F_4^{2-}$ and $UO_2Cl_4^{2-}$. From the dianion to monoanion, the U–F bond length is decreased significantly by 0.123 Å,[17] while the U–Cl bond length is only shortened by about 0.045 Å (Table II). This large difference in the U–F and U–Cl bonds upon electron detachment from the two uranyl tetrahalide complexes can be understood from both the intramolecular Coulomb repulsion and the nature of the HOMO, from which the electron is removed. The ground state of $UO_2F_4^{-}$ corresponds to the removal of an electron from the a_{2u} orbital of $UO_2F_4^{2-}$, which represents anti-bonding interactions between the F 2*p* and the UO_2^{2+} σ_u orbital. Hence, in addition to the reduced intramolecular Coulomb repulsion, the U–F bond is significantly enhanced by gaining more equatorial bonding character. In contrast, the ground state of the monoanion $UO_2Cl_4^{-}$ corresponds to the removal of an electron from the nonbonding a_{2g} orbital, which is of pure Cl 3*p* character (Fig. 3). Hence, it is expected that the U–Cl bond lengths should not be affected significantly in the monoanion.

C. Influence of U–O bonding by equatorial ligands: Cl^- vs. F^-

Upon electron detachment, the axial U–O bonding in $UO_2Cl_4^{-}$ is not significantly changed (Table I), and the same was observed in $UO_2F_4^{-}$.[17] The U–O bond length in $UO_2F_4^{2-}$ is slightly longer in the gas phase (1.83 Å) (Ref. 17) than that in solution (1.800 Å) (Ref. 19 and 64) or in solid (1.780 Å).[65] For $UO_2Cl_4^{2-}$, the calculated U–O bond length is 1.76 Å (Table I), which is close to the result of 1.774 Å from the crystal structure of $CsUO_2Cl_4$.[21] These observations can be understood by the different equatorial ligand bonding in $UO_2F_4^{2-}$ and $UO_2Cl_4^{2-}$. In the previous

study of $UO_2F_4^{2-}$,[17] we found that its frontier MOs show π-interactions between the U $5f_\pi$ orbital and the equatorial ligands. Denning suggested that this π-interaction renders the U–F bonds in $UO_2F_4^{2-}$ some multiple bonding characters.[1,7] This observation is consistent with the U–F bonding in UF_6 (1.996 Å), which is also suggested to possess multiple bonding characters.[66,67] At this short equatorial distance, the F $2p$ orbitals can have better interactions with the U–O orbitals, as reflected in the frontier MOs of $UO_2F_4^{2-}$. However, the strong electrostatic repulsion from the F^- ligands can destabilize the U–O bonding. In the condensed phase, the solvent or counter cations alleviate the intramolecular Coulomb repulsion effects on the U–O bonds within $UO_2F_4^{2-}$. In the gas phase, the intramolecular Coulomb repulsion can fully exert its influence on the U–O bonds. For the case of $UO_2Cl_4^{2-}$, the third-row non-metal elements in the periodic table cannot efficiently form multiple bonds with U because of the Pauli repulsion from the inner shell orbitals. Hence, at the equatorial distance of 2.73 Å, there is a smaller net overlap between Cl $3p$ and the MOs of the UO_2^{2+} moiety. Consequently, the U–O bonds are not affected significantly from the intramolecular Coulomb repulsion in the gas phase.

VII. CONCLUSIONS

We report the observation and characterization of the doubly charged $UO_2Cl_4^{2-}$ anion in the gas phase. Photoelectron spectroscopy and *ab initio* CCSD(T) theoretical calculations are used to probe the stability of $UO_2Cl_4^{2-}$ and its electronic structure. The $UO_2Cl_4^{2-}$ dianion is observed to have high electronic stability with an adiabatic electron detachment energy of 2.40 eV. Theoretical calculations show that the frontier MOs of $UO_2Cl_4^{2-}$ are mainly composed of Cl $3p$ orbitals. The simulated spectrum at the CCSD(T) level is found to be in good agreement with the experimental data. The comparison of $UO_2Cl_4^{2-}$ with $UO_2F_4^{2-}$ reveals interesting differences due to their different electrostatic interactions between the uranyl and the halide ligands. The much higher electron detachment energy of $UO_2Cl_4^{2-}$ relative to $UO_2F_4^{2-}$ is largely a result of its larger size and reduced intramolecular Coulomb repulsion, as well as the stronger uranyl-F interaction in the latter. The gas-phase PES results of uranyl complexes provide ideal experimental data for benchmarking theoretical methodologies of relativistic quantum chemistry involving strong electron correlations.

ACKNOWLEDGMENTS

This work was supported by the U.S. Department of Energy (DOE), Office of Basics Energy Sciences, Heavy Element Chemistry Program, under Grant No. DE-FG02-11ER16261 (P. D. Dau, H. T. Liu, and L. S. Wang). The theoretical work was supported by NKBRSF (2011CB932400) and the National Science Foundation of China (NSFC) (20933003, 11079006, 91026003) (J. Su and J. Li). The calculations were performed using the DeepComp 7000 computer at the Supercomputer Center of the Computer Network Information Center, Chinese Academy of Sciences, and the Shanghai Supercomputing Center.

[1] R. G. Denning, Struct. Bonding **79**, 215 (1992).
[2] M. V. Ryzhkov and V. A. Gubanov, J. Radioanal. Nucl. Chem. **143**, 85 (1990).
[3] P. A. Tanner, J. Chem. Soc., Faraday Trans. 2 **80**, 365 (1984).
[4] T. J. Barker, R. G. Denning, and J. R. G. Thorne, Inorg. Chem. **31**, 1344 (1992).
[5] N. B. Borkovskii and A. M. Lyudchik, Dokl. Akad. Nauk. Belarusi **29**, 137 (1985).
[6] L. R. Morss, N. M. Edelstein, and J. Fuger, *The Chemistry of the Actinide and Transactinide Elements* (Springer, Dordrecht, NLD, 2006), Vol. 1.
[7] R. G. Denning, J. Phys. Chem. A **111**, 4125 (2007).
[8] S. P. Mcglynn and J. K. Smith, J. Mol. Spectrosc. **6**, 164 (1961).
[9] M. Pepper and B. E. Bursten, Chem. Rev. **91**, 719 (1991).
[10] Z. Y. Zhang and R. M. Pitzer, J. Phys. Chem. A **103**, 6880 (1999).
[11] R. G. Denning and I. D. Morrison, Chem. Phys. Lett. **180**, 101 (1991).
[12] S. Matsika and R. M. Pitzer, J. Phys. Chem. A **105**, 637 (2001).
[13] R. G. Denning, J. C. Green, T. E. Hutchings, C. Dallera, A. Tagliaferri, K. Giarda, N. B. Brookes, and L. Braicovich, J. Chem. Phys. **117**, 8008 (2002).
[14] K. Servaes, C. Hennig, R. Van Deun, and C. Gorller-Walrand, Inorg. Chem. **44**, 7705 (2005).
[15] V. V. Zhurov, E. A. Zhurova, and A. A. Pinkerton, Inorg. Chem. **50**, 6330 (2011).
[16] J. Su, K. Zhang, W. H. E. Schwarz, and J. Li, Inorg. Chem. **50**, 2082 (2011).
[17] P. D. Dau, J. Su, H. T. Liu, J. B. Liu, D. L. Huang, J. Li, and L. S. Wang, Chem. Sci. **3**, 1137 (2012).
[18] F. Ruiperez and U. Wahlgren, J. Phys. Chem. A **114**, 3615 (2010).
[19] V. Vallet, U. Wahlgren, B. Schimmelpfennig, H. Moll, Z. Szabo, and I. Grenthe, Inorg. Chem. **40**, 3516 (2001).
[20] T. J. Barker, R. G. Denning, and J. R. G. Thorne, Inorg. Chem. **26**, 1721 (1987).
[21] D. J. Watkin, R. G. Denning, and K. Prout, Acta Crystallogr. C: Cryst. Struct. Commun. **47**, 2517 (1991).
[22] C. Gorller-Walrand, S. De Houwer, L. Fluyt, and K. Binnemans, Phys. Chem. Chem. Phys. **6**, 3292 (2004).
[23] C. Hennig, K. Servaes, P. Nockemann, K. Van Hecke, L. Van Meervelt, J. Wouters, L. Fluyt, C. Gorller-Walrand, and R. Van Deun, Inorg. Chem. **47**, 2987 (2008).
[24] L. Soderholm, S. Skanthakumar, and R. E. Wilson, J. Phys. Chem. A **115**, 4959 (2011).
[25] V. V. Zhurov, E. A. Zhurova, A. I. Stash, and A. A. Pinkerton, J. Phys. Chem. A **115**, 13016 (2011).
[26] P. Tecmer, R. Bast, K. Ruud, and L. Visscher, J. Phys. Chem. A **116**, 7397 (2012).
[27] M. Buhl, N. Sieffert, and G. Wipff, Chem. Phys. Lett. **467**, 287 (2009).
[28] E. van Besien, K. Pierloot, and C. Gorller-Walrand, Phys. Chem. Chem. Phys. **8**, 4311 (2006).
[29] G. K. Liu, J. Phys. Chem. A **115**, 12419 (2011).
[30] K. Pierloot and E. van Besien, J. Chem. Phys. **123**, 204309 (2005).
[31] K. Pierloot, E. van Besien, E. van Lenthe, and E. J. Baerends, J. Chem. Phys. **126**, 194311 (2007).
[32] J. Su, W. H. E. Schwarz, and J. Li, Inorg. Chem. **51**, 3231 (2012).
[33] G. S. Groenewold, M. J. van Stipdonk, J. Oomens, W. A. de Jong, G. L. Gresham, and M. E. McIlwain, Int. J. Mass Spectrom. **297**, 67 (2010).
[34] L. S. Wang, C. F. Ding, X. B. Wang, and S. E. Barlow, Rev. Sci. Instrum. **70**, 1957 (1999).
[35] H. T. Liu, Y. L. Wang, X. G. Xiong, P. D. Dau, Z. Piazza, D. L. Huang, C. Q. Xu, J. Li, and L. S. Wang, "The Electronic Structure and Chemical Bonding in Gold Dihydride: AuH_2^- and AuH_2," Chem. Sci., submitted.
[36] C. G. Ning, X. G. Xiong, Y. L. Wang, J. Li, and L. S. Wang, Phys. Chem. Chem. Phys. **14**, 9323 (2012).
[37] J. P. Perdew, K. Burke, and M. Ernzerhof, Phys. Rev. Lett. **77**, 3865 (1996).
[38] C. Lee, W. Yang, and R. G. Parr, Phys. Rev. B **37**, 785 (1988).
[39] See http://www.scm.com for ADF2010.01, SCM, Theoretical Chemistry, Vrije Universiteit, Amsterdam, The Netherlands.
[40] C. F. Guerra, J. G. Snijders, G. te Velde, and E. J. Baerends, Theor. Chem. Acc. **99**, 391 (1998).
[41] G. T. Velde, F. M. Bickelhaupt, E. J. Baerends, C. F. Guerra, S. J. A. Van Gisbergen, J. G. Snijders, and T. Ziegler, J. Comput. Chem. **22**, 931 (2001).
[42] E. Van Lenthe and E. J. Baerends, J. Comput. Chem. **24**, 1142 (2003).

[43]E. Vanlenthe, E. J. Baerends, and J. G. Snijders, J. Chem. Phys. **99**, 4597 (1993).
[44]H. J. Werner, P. J. Knowles, R. Lindh, F. R. Manby, M. Schuütz *et al.*, MOLPRO, version 2008.1, a package of *ab inito* programs, 2008, see http://www.molpro.net.
[45]X. B. Wang, Y. L. Wang, J. Yang, X. P. Xing, J. Li, and L. S. Wang, J. Am. Chem. Soc. **131**, 16368 (2009).
[46]Y. L. Wang, X. B. Wang, X. P. Xing, F. Wei, J. Li, and L. S. Wang, J. Phys. Chem. A **114**, 11244 (2010).
[47]Y. L. Wang, H. J. Zhai, L. Xu, J. Li, and L. S. Wang, J. Phys. Chem. A **114**, 1247 (2010).
[48]J. Su, Y. L. Wang, F. Wei, W. H. E. Schwarz, and J. Li, J. Chem. Theory Comput. **7**, 3293 (2011).
[49]H. T. Liu, X. G. Xiong, P. D. Dau, Y. L. Wang, J. Li, and L. S. Wang, Chem. Sci. **2**, 2101 (2011).
[50]K. Kowalski and P. Piecuch, J. Chem. Phys. **120**, 1715 (2004).
[51]M. Valiev, E. J. Bylaska, N. Govind, K. Kowalski, T. P. Straatsma, H. J. J. Van Dam, D. Wang, J. Nieplocha, E. Apra, T. L. Windus, and W. de Jong, Comput. Phys. Commun. **181**, 1477 (2010).
[52]W. Küchle, M. Dolg, H. Stoll, and H. Preuss, J. Chem. Phys. **100**, 7535 (1994).
[53]See http://www.theochem.uni-stuttgart.de/pseudopotentials for the pseudopotential and basis sets of uranium.
[54]A. Nicklass, M. Dolg, H. Stoll, and H. Preuss, J. Chem. Phys. **102**, 8942 (1995).
[55]X. Y. Cao and M. Dolg, J. Mol. Struc.: THEOCHEM. **673**, 203 (2004).
[56]R. A. Kendall, T. H. Dunning, and R. J. Harrison, J. Chem. Phys. **96**, 6796 (1992).
[57]D. E. Woon and T. H. Dunning, J. Chem. Phys. **98**, 1358 (1993).
[58]F. Wei, G. S. Wu, W. H. E. Schwarz, and J. Li, Theor. Chem. Acc. **129**, 467 (2011).
[59]L. S. Wang, X. B. Wang, and C. F. Ding, Phys. Rev. Lett. **81**, 3351 (1998).
[60]X. B. Wang, C. F. Ding, and L. S. Wang, Chem. Phys. Lett. **307**, 391 (1999).
[61]The $UO_2Cl_3^-$ anion can also be produced directly by ESI. We measured its photoelectron spectrum at 157 nm and found its ADE to be more than 6.5 eV.
[62]X. B. Wang, Y. L. Wang, H. K. Woo, J. Li, G. S. Wu, and L. S. Wang, Chem. Phys. **329**, 230 (2006).
[63]E. van Lenthe, J. G. Snijders, and E. J. Baerends, J. Chem. Phys. **105**, 6505 (1996).
[64]M. Straka, K. G. Dyall, and P. Pyykko, Theor. Chem. Acc. **106**, 393 (2001).
[65]T. C. W. Mak and W. H. Yip, Inorg. Chim. Acta **109**, 131 (1985).
[66]M. Straka, M. Patzschke, and P. Pyykko, Theor. Chem. Acc. **109**, 332 (2003).
[67]F. Wei, G. S. Wu, W. H. E. Schwarz, and J. Li, J. Chem. Theory Comput. **7**, 3223 (2011).